Statistical Analysis to Develop a Three-Dimensional Surface Model of a Midsize-Male Foot

Matthew P. Reed
Sheila M. Ebert
Brian D. Corner

October 2013

UMTRI
UNIVERSITY OF MICHIGAN
TRANSPORTATION
RESEARCH INSTITUTE

Statistical Analysis to Develop a Three-Dimensional
Surface Model of a Midsize-Male Foot

Final Report

by

Matthew P. Reed
Sheila M. Ebert

University of Michigan Transportation Research Institute

Brian D. Corner
U.S. Army Natick Soldier Research, Development, and Engineering Center

UMTRI-2013-19

October 2013

REPORT DOCUMENTATION PAGE

1. REPORT DATE (DD-MM-YYYY) October 31, 2013	2. REPORT TYPE Final Report	3. DATES COVERED (From - To) January 2013– June 2013

4. TITLE AND SUBTITLE		
Statistical Analysis to Develop a Three-Dimensional Surface Model of a Midsize-Male Foot	5a. CONTRACT NUMBER	
	5b. GRANT NUMBER	
	5c. PROGRAM ELEMENT NUMBER	

6. AUTHOR(S)		
Reed, Matthew P., Ebert, Sheila M., and Corner, Brian D.	5d. PROJECT NUMBER	
	5e. TASK NUMBER	
	5f. WORK UNIT NUMBER	

7. PERFORMING ORGANIZATION NAME(S) AND ADDRESS(ES)	8. PERFORMING ORGANIZATION REPORT
University of Michigan Transportation Research Institute	UMTRI-2013-19

9. SPONSORING / MONITORING AGENCY NAME(S) AND ADDRESS(ES)	10. SPONSOR/MONITOR'S ACRONYM(S)
US Army Tank Automotive Research, Development, and Engineering Center Warren, MI 48397-5000	
	11. SPONSOR/MONITOR'S REPORT NUMBER(S) Issued Upon Submission

12. DISTRIBUTION / AVAILABILITY STATEMENT

Approved for unlimited public release, US Army TARDEC

13. SUPPLEMENTARY NOTES

14. ABSTRACT
A representative midsize-male foot was generated via a statistical analysis of foot scans from 107 men with widely varying body size. Seventy-two surface landmarks were manually extracted from the original scan data. A template fitting method was used to represent each scan with a homologous mesh. A principal component analysis and least-squares linear regression were used to generate a foot surface model with landmarks using a reference stature of 1755 mm and a body mass of 83.19 kg. The statistical model can be used to generate a wide range of male foot sizes and shapes.

15. SUBJECT TERMS
Anthropometry, Posture, Vehicle Occupants, Statistical Shape Analysis, Safety

16. SECURITY CLASSIFICATION OF: Unclassified: Dist. A: Approved for public release			17. LIMITATION OF ABSTRACT	18. NUMBER OF PAGES	19a. NAME OF RESPONSIBLE PERSON M.P. Reed
a. REPORT UNCLAS	b. ABSTRACT UNCLAS	c. THIS PAGE UNCLAS		26	19b. TELEPHONE NUMBER (include area code) (734)936-1111

ACKNOWLEDGMENTS

Disclaimer: Reference herein to any specific commercial company, product, or service by trade name, trademark, manufacturer, or otherwise, does not necessarily constitute or imply its endorsement, recommendation, or favoring by the United States Government or the Department of the Army (DoA). The opinions of the auothers expressed herein do not necessarily state or reflect those of the United States Government or the DoA, and shall not be used for advertising or product endorsement purposes.

CONTENTS

EXECUTIVE SUMMARY

A representative midsize-male foot was generated via a statistical analysis of foot scans from 107 men with widely varying body size. Seventy-two surface landmarks were manually extracted from the original scan data. A template fitting method was used to represent each scan with a homologous mesh. A principal component analysis and least-squares linear regression were used to generate a foot surface model with landmarks using a reference stature of 1755 mm and a body mass of 83.19 kg. The statistical model can be used to generate a wide range of male foot sizes and shapes.

INTRODUCTION

Three-dimensional anthropometry has been widely applied to foot measurement. Statistical models of foot size and shape based on scan data have been used for custom footwear design and the development of improved shoe lasts (Goonetilleke 2013). The primary objective of the current effort was to develop a foot specification for the Warrior Injury Assessment Manikin (WIAMan), an anthropomorphic test device being developed by the U.S. Army for vehicle and seat testing in underbody blast scenarios. WIAMan is intended to represent a midsize male soldier, with stature of 1755 mm and body mass of 83.19 kg, selected as the median values in Paquette et al. (2009).

Most ATD feet have generic shapes scaled for length and width but lacking anatomical detail. For example, the MIL-LX leg, shown in Figure 1, uses the midsize-male Hybrid-III foot. The foot is shaped to accommodate a curved footbed in a shoe and lacks well-defined anatomical landmarks.

The current study took advantage of recent advancements in both measurement technology and analysis methods. A sample of foot scans was drawn from a much larger study of soldier anthropometry. The locations of a set of landmarks were extracted from each scan. A template mesh was fitted to each scan to enable statistical analysis, and a regression approach was used to calculate a surface mesh representing the average foot for men with the reference stature and body mass for WIAMan.

Figure 1. MIL-LX, which uses the midsize-male Hybrid-III foot (Humanetics Innovative Solutions).

METHODS

Data Source

Surface scans of the right feet of 107 men with a wide range of body size were obtained using a InFoot scanner (I-Ware Laboratory) as part of the ANSUR II study (Hotzman et al. 2011). The scans were taken with the men standing with their weight distributed approximately evenly across both feet. The scanner obtains the shape of the plantar surface of the foot by scanning through a glass surface.

Landmark Location Extraction

The data were obtained as unstructured polygon meshes with approximately 100,000 vertices. A set of surface landmarks shown in Figure 2 and listed in Appendix A were extracted from every scan using manual methods in MeshLab software.
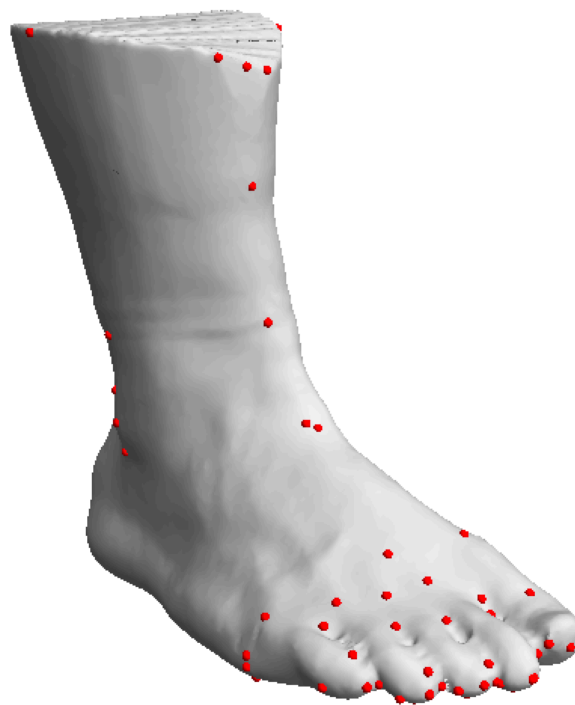

Figure 2. Surface landmarks illustrated on an exemplar scan.

Surface Data Processing

Using an automated script in MeshLab software (http://meshlab.sourceforge.net/), each scan was decimated to 25,004 vertices using the quadric edge collapse decimation filter. Filter options were set as follows: quality threshold 0.3, optimal positioning of simplified vertices, and post-simplification cleaning. The resulting meshes were stored in a polygonal format with vertex normals calculated by averaging the orientations of each adjacent face. A template with 25,004 vertices was created from an exemplar scan. Using custom software, the template was then fit to each scan through a two-step procedure:

1. A radial-basis function morphing method similar to the method described by Bennink et al. (2006) with a Hardy norm and a parameter value of 10 mm was used to morph the template to match the scan at each of the landmark locations.
2. An implicit surface fitting method adapted from Carr et al. (2001) was used to fit the template mesh to the scan data.

Figure 3 illustrates these steps. Following template fitting, each scan was represented by a set of homologous landmarks and 25,004 vertices of the template, each lying at homologous anatomical locations.
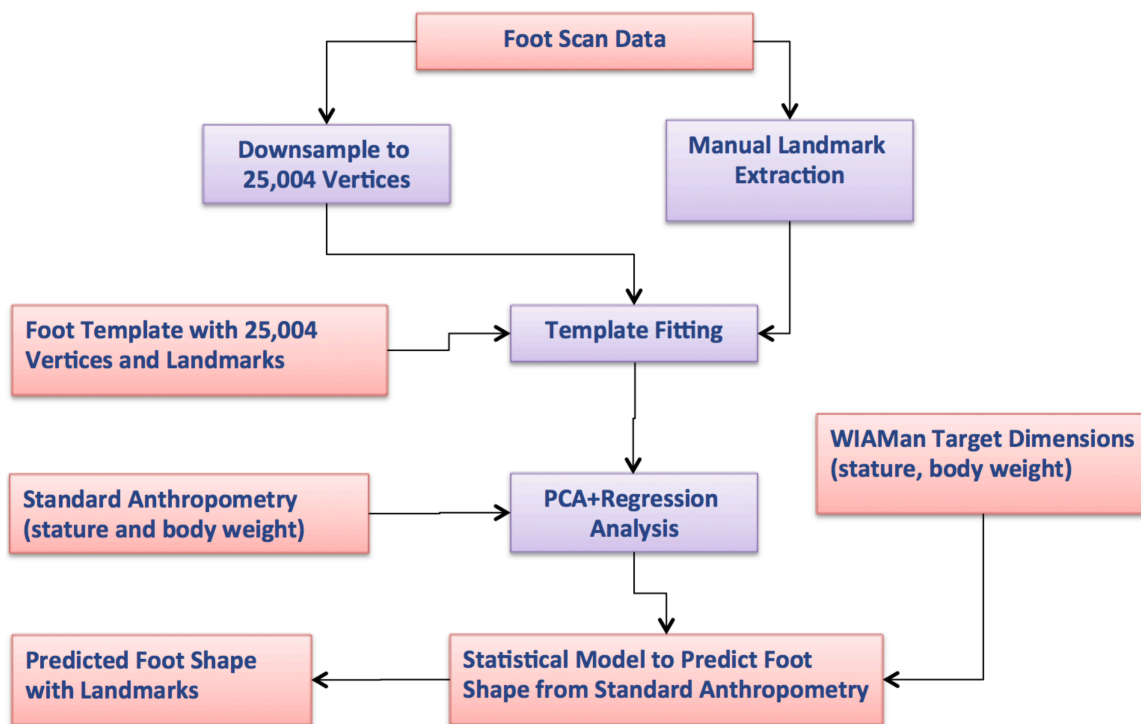

Figure 3. Data processing and analysis flowchart.

Surface Data Analysis

Using methods previously applied to modeling of a wide range of anatomical structures (Allen et al. 2003, Reed and Parkinson 2008, Reed et al. 2009), a principal component analysis (PCA) was performed using custom software. First, a Procrustes alignment of the landmarks was conducted to remove differences in posture, particularly rotation about the vertical axis. The transformations from the Procrustes analysis were then applied to all vertices on the foot meshes. Second, a PCA was conducted on the combined landmarks and mesh vertices. Finally, a least-squares linear regression analysis was conducted, using 60 principal components (PCs,) which accounted for 98 percent of the variance in the mesh vertices and landmarks. The selection of 60 PCs struck a balance between surface detail and model smoothness. The resulting regression model was used to predict the landmark and vertex locations as a function of stature and body mass index (body weight in kg divided by stature in meters squared, kg/m^2).

RESULTS

Sample Anthropometry

Figures 4 and 5 show the distribution of stature, BMI, foot length, and foot width for the study population. Table 1 shows summary statistics.
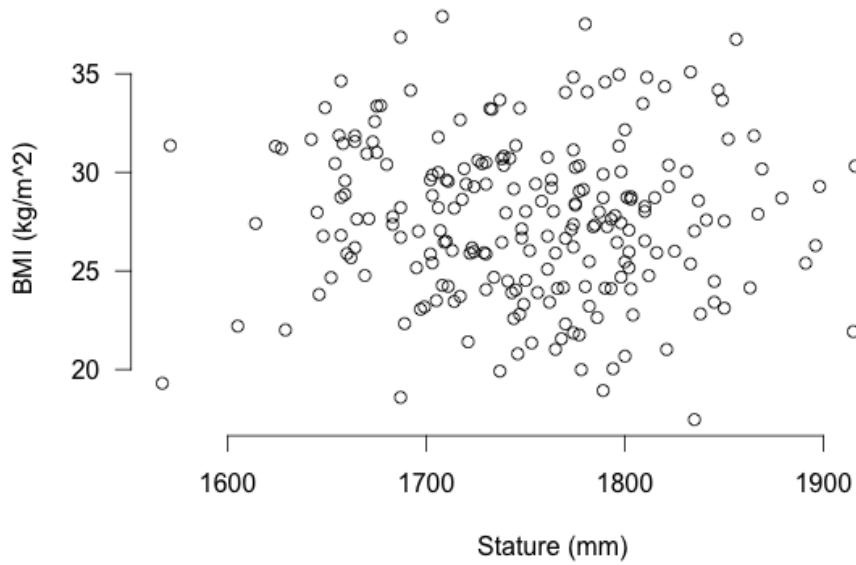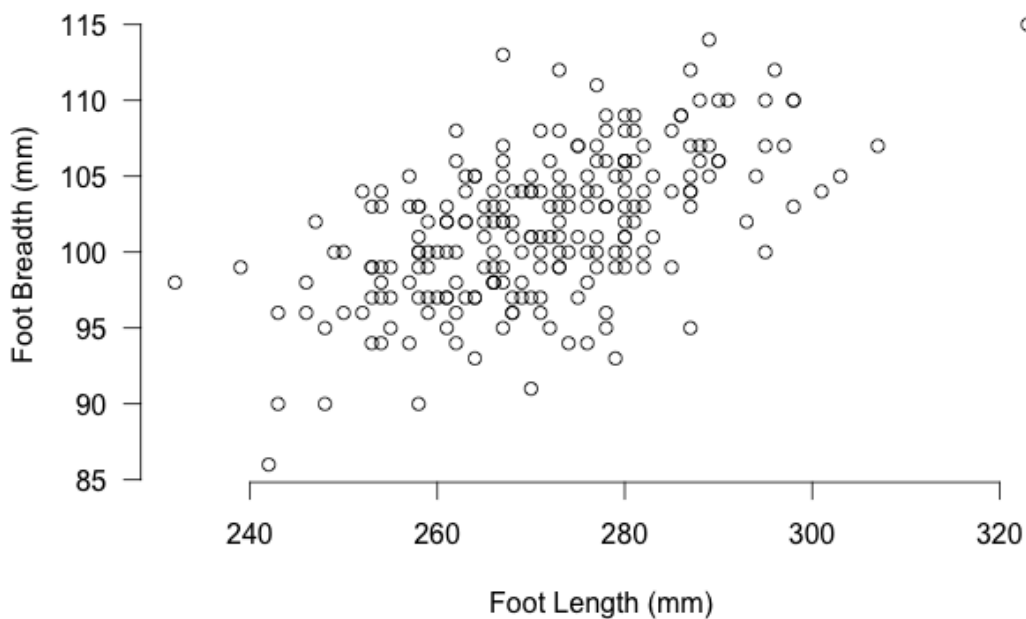

Figure 4. BMI by stature.

Figure 5. Foot breadth by foot length.

Table 1
Summary Statistics for Standard Anthropometric Measures

Dimension (mm, kg)	Mean	SD
Stature	1755	71.1
Body Weight (kg)	85.2	13.9
Foot Length	271	13.6
Foot Breadth	102	4.9

Repeatability of Landmark Extraction

The landmarks listed in Appendix A were digitized on eight scans by 2 experimenters and the landmarks on 2 scans were digitized by 3 experimenters. The standard deviations of the location coordinates were calculated on each axis. Across axes and scans, the mean standard deviation for all points was 2.21 mm. One experimenter digitized one scan three times. The mean standard deviation was 1.53 mm.

Principal Component Analysis

Figure 6 illustrates the first 6 PCs, which together account for 88% of the variance (variance fractions 0.38, 0.27, 0.11, 0.06, 0.04, 0.02, respectively). As expected, the first PC is primarily related to foot size, particularly length. The second PC shows a posture difference related to ankle flexion/extension. The third PC is related to arch height and the fourth to ankle/calf circumference. The fifth and sixth PCs do not have a readily apparent interpretation.
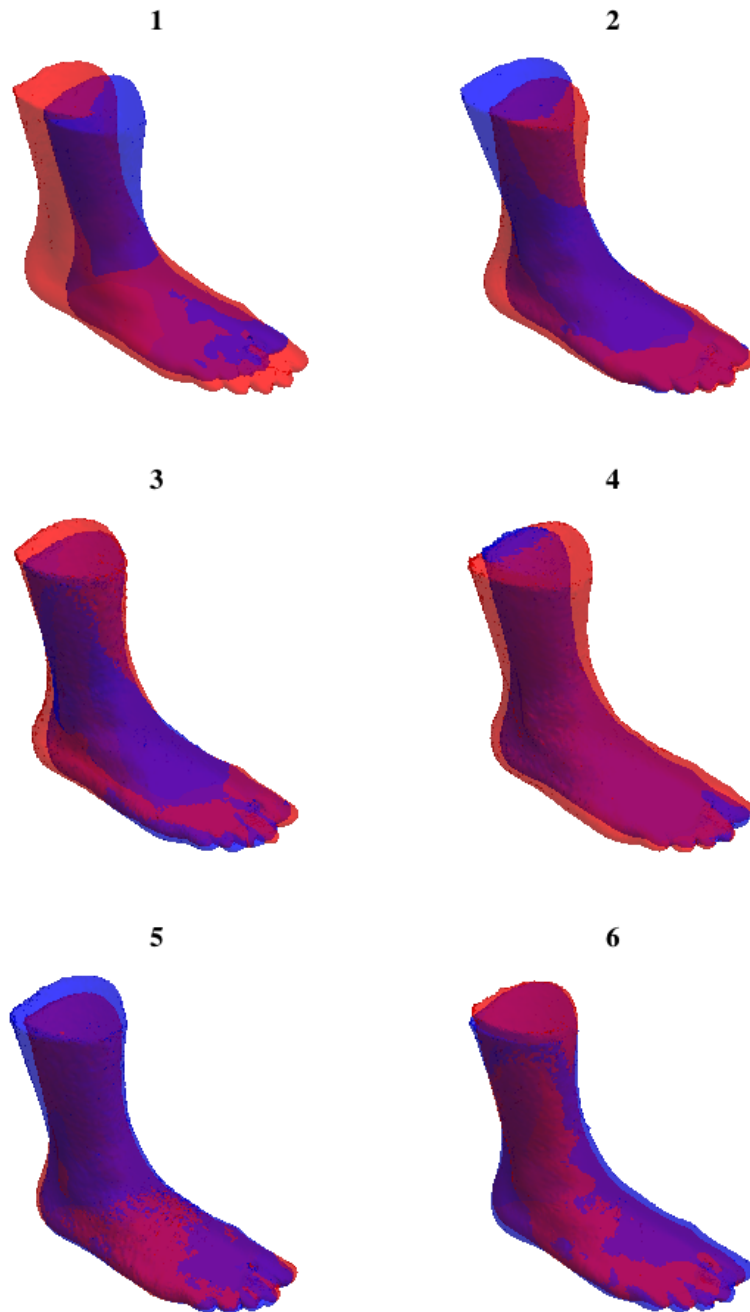

Figure 6. Illustration of ±3 SD on the first six principal components.

Midsize-Male Foot

Figure 7 shows the midsize-male foot generated from the regression model using of the reference stature and body weight of 1755 mm and 83.19 kg. Appendix B lists the predicted landmark locations.
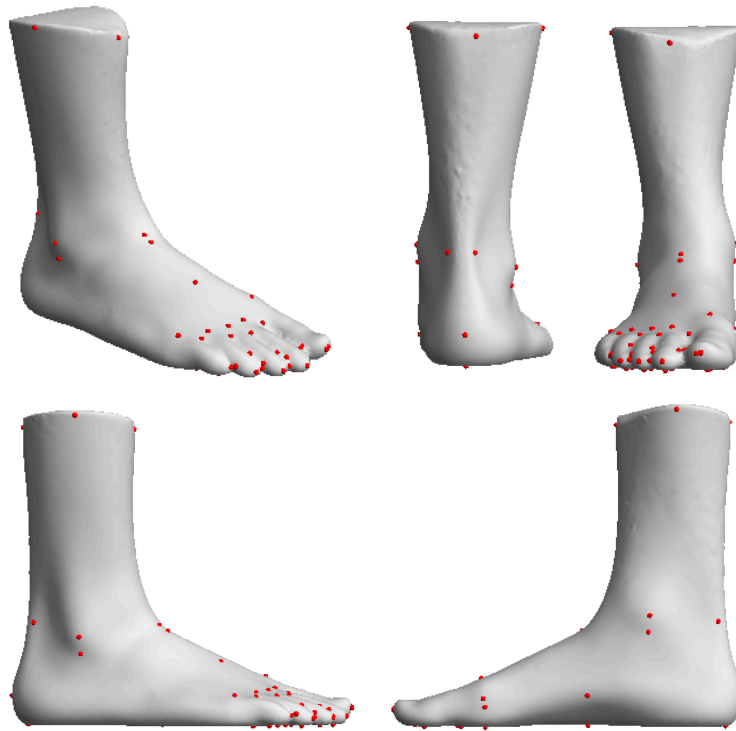

Figure 7. Midsize-male foot generated by regression analysis.

DISCUSSION

Accomplishments

A statistical model of male foot geometry was created using a sample of young male feet. A large number of landmarks were manually extracted from each scan, enabling a high level of homology to be preserved during template fitting. The PCA plus regression approach used in this work is an effective, widely used method for generating predictions. The resulting model can be used to predict foot shape as a function of foot size or to predict foot size and shape as a function of overall body dimensions. For example, the model could be used to predict the average foot shape for an individual with 95th-percentile stature, or the foot shape for a person with 95th-percentile foot width and length. The use of 60 PCs for generating the midsize-male foot strikes a balance between surface smoothing and preserving fine details.

Limitations

The sample size is the primary limitation of this work, although the analysis conducted here is based on a diverse sample of feet from men with a wide range of body size. A sample of 1000 feet would provide more confidence in estimating the shapes of small or large feet. All of the subjects were drawn from the U.S. Army population, and hence the data may not be representative of other populations. In particular, older civilian populations may have different foot shapes. The foot scans were obtained from standing subject bearing approximately half of their body weight on the scanned foot, which rested on a flat platform. A foot supporting less weight, or a foot in a shoe, would be expected to have a different shape.

As with any regression model, predictions near the center of the distribution of independent variables will be more precise than those in the tails of the distribution. In this case, the target dimensions are very close to the mean, so the precision is very similar to taking a simple average. Using the sample size of 107, the values in Table 1 can be used to compute standard error of the mean for foot length and width of 1.4 mm and 0.5 mm, respectively. The precision of the prediction of any particular dimension of the foot generated by the model is in this range.

The manual landmark extraction process introduces the potential for bias and random variance. Some landmarks relating to bony prominences would be easier to locate on a live subject, using palpation. The scan quality was high on the boundaries of the feet, but obscuration between the toes led to some uncertainty in landmark locations in those areas. Many of the landmarks used in this study are primarily useful for template fitting. Only a fraction of these, and primarily those related to bony landmarks, would be appropriate for use in developing the specification for a physical foot model.

The scanning methodology introduced noise and surface corruption into the data from the lower shank. Consequently, the model validity extends only 125 mm above the sole rest surface.

The analysis method provides flexibility in generating representative male feet. For example, the foot could be predicted using target length and width, rather than overall body dimensions. Near the center of the distribution, the differences are small, but, for example, a 95th-percentile foot by length would be markedly different than the foot for a man 95th-percentile by stature. Both can be generated using the model developed in this research.

REFERENCES

Allen, B., Curless, B., and Popovic, Z. (2003). The space of human body shapes: reconstruction and parameterization from range scans. *Proceedings of the 2003 International Conference on Computer Graphics and Interactive Techniques (SIGGRAPH).* San Diego, CA.

Bennink, H.E., Korbeeck, J.M., Janssen, B.J., and Romenij, B.M. (2006). Warping a neuro-anatomy atlas on 3D MRI data with radial basis functions. *Proceedings of the 2006 International Conference on Biomedical Engineering.* pp. 214-218.

Carr, J.C., Beatson, R.K., Cherrie, J.B., Mitchell, T.J., Fright, W.R., McCallum, B.C., and Evans, T.R. (2001). Reconstruction and representation of 3D objects with radial basis functions. *SIGGRAPH 01: Proceedings of the 28th Annual Conference on Computer Graphics and Interactive Techniques.* ACM.

Goonetilleke, R.S. (2013). *The Science of Footwear.* CRC Press, Boca Raton.

Hotzman, J., Gordon, C.C., Bradtmiller, B., Corner, B.D., Mucher, M., Kristensen, S., Paquette, S., and Blackwell, C.L. (2011). Measurer's Handbook: U.S. Army and Marine Corps Anthropometric Surveys. Technical Report NATICK/TR-11/017. U.S. Army Natick Soldier RD&E Center.

Paquette, S., Gordon, C.,and Bradtmiller, B. (2009). Anthropometric Survey (ANSUR) II Pilot Study: Methods and Summary Statistics. Technical Report NATICK/TR-09/014. U.S. Army Natick Soldier Research, Development, and Engineering Center, Natick, MA.

Reed, M.P., Sochor, M.M., Rupp, J.D., Klinich, K.D., and Manary, M.A. (2009). Anthropometric specification of child crash dummy pelves through statistical analysis of skeletal geometry. *Journal of Biomechanics,* 42:1143-1145.

Reed, M.P. and Parkinson, M.B. (2008). Modeling variability in torso shape for chair and seat design. DETC2008-49483. *Proceedings of the ASME Design Engineering Technical Conferences.* ASME, New York.

APPENDIX A
Surface Landmark Definitions

Table A1
Point List

	Meshlab Point Name	Point Description
1	Malleolus_Lateral	Lateral Malleolus
2	Sphyrion_Fibulare	Sphyrion Fibulare
3	5th_Metatarsal-Phalangeal_Protrsn	5th Metatarsal-Phalangeal Protrusion
4	5th_Metatarsal-Phalangeal_Protrsn_Floor	Foot-floor breakaway point at 5th metatarsal-phalangeal protrusion proximal-distal location
5	Malleolus_Medial	Medial Malleolus
6	Sphyrion_Tibulare	Syphyrion Tibulare
7	1st_Metatarsal-Phalangeal_Protrsn	1st Metatarsal-Phalangeal Protrusion
8	1st_Metatarsal-Phalangeal_Protrsn_Floor	Foot-floor breakaway point at 1st metatarsal-phalangeal protrusion proximal-distal location
9	1st_Phlngs_Pododactylion	1st Phalanges Pododactylion
10	2nd_Phlngs_Pododactylion	2nd Phalanges Pododactylion
11	3rd_Phlngs_Pododactylion	3rd Phalanges Pododactylion
12	4th_Phlngs_Pododactylion	4th Phalanges Pododactylion
13	5th_Phlngs_Pododactylion	5th Phalanges Pododactylion
14	1_2_Phlngs_Distal_Indent	Indent between 1st and 2nd Distal Phalanges *
15	2_3_Phlngs_Distal_Indent	Indent between 2nd and 3rd Distal Phalanges
16	3_4_Phlngs_Distal_Indent	Indent between 3rd and 4th Distal Phalanges
17	4_5_Phlngs_Distal_Indent	Indent between 4th and 5th Distal Phalanges
18	5^{th}_Phlngs_MidDistJnt_Lat	
19	5^{th}_Phlngs_MidDistJnt_Med	
20	4^{th}_Phlngs_MidDistJnt_Lat	
21	4^{th}_Phlngs_MidDistJnt_Med	Medial and lateral points on joint between mid and distal segment of phalanges 5- 2, as close to mid joint height of each phalange as possible
22	3^{rd}_Phlngs_MidDistJnt_Lat	
23	3^{rd}_Phlngs_MidDistJnt_Med	
24	2^{nd}_Phlngs_MidDistJnt_Lat	
25	2^{nd}_Phlngs_MidDistJnt_Med*	
26	1^{st}_Phlngs_2ndMidDistJnt_Lat*	Lateral point on 1st phalanges at the same distal-proximal position as 2^{nd}_Phlngs_MidDistJnt_Med, also as close to the height of this point as possible
27	1^{st}_Phlngs_ProxDistJnt_Med	Medial point on the joint between the proximal-distal joint of the 1st phalanges as close to the mid joint height as possible
28	1_2_Phlngs_Gap_Distal	Most distal point in hole-type gap between 1st and 2nd phalanges, as inferior as possible*
29	1_2_Phlngs_Gap_Proximal	Most proximal point in hole-type gap between 1st and 2nd phalanges, as inferior as possible*
30	1_2_Phlngs_DorsalProximal_Indent	Most dorsal-proximal point between 1st and 2nd phalanges
31	2_3_Phlngs_DorsalProximal_Indent	Most dorsal-proximal point between 2nd and 3rd phalanges
32	3_4_Phlngs_DorsalProximal_Indent	Most dorsal-proximal point between 3rd and 4th phalanges
33	4_5_Phlngs_DorsalProximal_Indent	Most dorsal-proximal point between 4th and 5th phalanges
34	1st_Metatarsal-Phalangeal_MaxSuperior	Most superior point on 1st metatarsal-phalangeal joint
35	2nd_Metatarsal-Phalangeal_MaxSuperior	Most superior point on 2nd metatarsal-phalangeal joint
36	3rd_Metatarsal-Phalangeal_MaxSuperior	Most superior point on 3rd metatarsal-phalangeal joint
37	4th_Metatarsal-Phalangeal_MaxSuperior	Most superior point on 4th metatarsal-phalangeal joint
38	5th_Metatarsal-Phalangeal_MaxSuperior	Most superior point on 5th metatarsal-phalangeal joint
39	1st_PhlngsDistSeg_Center_Floor	Center of floor contact point of the 1st distal phalanges
40	2nd_PhlngsDistSeg_Center_Floor	Center of floor contact point of the 2nd distal phalanges
41	3rd_PhlngsDistSeg_Center_Floor	Center of floor contact point of the 3rd distal phalanges
42	4th_PhlngsDistSeg_Center_Floor	Center of floor contact point of the 4th distal phalanges
43	5th_PhlngsDistSeg_Center_Floor	Center of floor contact point of the 5th distal phalanges

	Meshlab Point Name	Point Description
44	1st_Phlngs_BOF_Distal_Floor	Foot-floor breakaway point of ball-of-foot at the midline of the 1st phalanges
45	2nd_Phlngs_BOF_Distal_Floor	Foot-floor breakaway point of ball-of-foot at the midline of the 2nd phalanges
46	3rd_Phlngs_BOF_Distal_Floor	Foot-floor breakaway point of ball-of-foot at the midline of the 3rd phalanges
47	4th_Phlngs_BOF_Distal_Floor	Foot-floor breakaway point of ball-of-foot at the midline of the 4th phalanges
48	5th_Phlngs_BOF_Distal_Floor	Foot-floor breakaway point of ball-of-foot at the midline of the 5th phalanges
49	Foot-Leg_DorsalJunction_AnkleMidline	Foot-leg dorsal junction (inflection point) at ankle midline
50	Foot_Dorsum_Superior	The superior point of the talus immediately anterior to the talo-cural joint
51	Arch_Superior_Point_DorsalJunctionX	Most superior point on the arch at the Foot_Dorsm_Superior (above)
52	Arch_Floor_DorsalJunctionX	Foot-floor breakaway point on the arch at the Foot_Dorsm_Superior (above)
53	TarsometatarsalJoint_ExtensorBrevis_AnkleMidline	The inflection point on the dorsum of the foot superior to the tarso-metatarsal joint at the distal margin of the extensor brevis muscle
54	Heel_Floor_Posterior	Foot-floor breakaway point most posterior on the heel
55	Pternion	Most posterior point on the heel
56	Calcaneal_MinimumBreadth_Medial	Point on medial side of calcaneal tendon at its minimum breadth
57	Calcaneal_MinimumBreadth_Lateral	Point on lateral side of calcaneal tendon at its minimum breadth
58	CuffInfEdge_AnkleMidline_Anterior	Anterior-inferior edge of long underwear cuff at midline of ankle
59	CuffInfEdge_MalleolusLateral	Interior edge of long underwear cuff superior to lateral malleolus
60	CuffInfEdge_AnkleMidline_Posterior	Posterior-inferior edge of long underwear cuff at midline of ankle
61	CuffInfEdge_MalleolusMedial	Interior edge of long underwear cuff superior to medial malleolus
62	Maximum_Toe_Height_Location**	Maximum toe height
63	Acropodian**	Most distal phalangeal point
64	WidthMaximum_Medial**	Most medial point on foot
65	WidthMaximum_Lateral**	Most lateral point on foot
66	CalfCutOff_Superior_Lateral	Superior-lateral point of leg cut-off
67	CalfCutOff_Superior_Posterior	Superior-posterior point of leg cut-off
68	CalfCutOff_Superior_Medial	Superior-medial point of leg cut-off
69	CalfCutOff_Superior_Anterior	Superior-anterior point of leg cut-off
70	CalfNoise_Anterior_Distal	The distal tip of the triangle-shaped noise on the leg anterior
71	CalfNoise_Anterior_Lateral***	The lateral point of the triangle-shaped noise on the leg anterior
72	CalfNoise_Anterior_Medial***	The medial point of the triangle-shaped noise on the leg anterior
73	CalfNoise_Posterior_Distal	The distal tip of the triangle-shaped noise on the leg posterior
74	CalfNoise_Posterior_Lateral***	The lateral point of the triangle-shaped noise on the leg posterior
75	CalfNoise_Posterior_Medial***	The medial point of the triangle-shaped noise on the leg posterior

* In some scans these points are in the same place.
** Changes in relative locations of these points will disrupt template fitting.
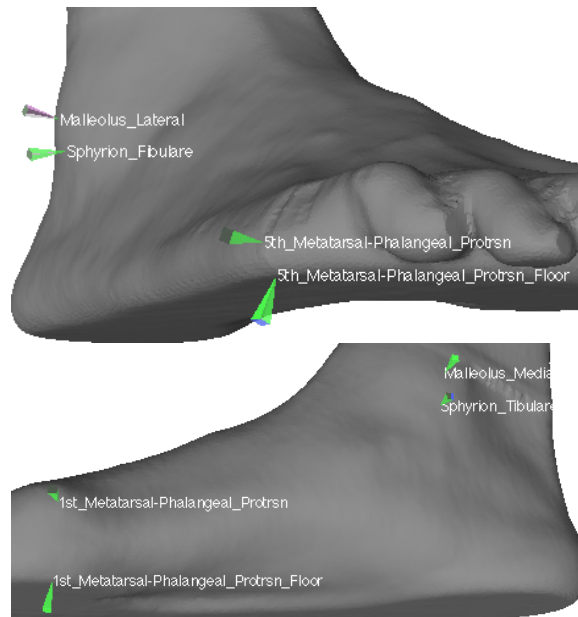*** Often at the calf-cut-off
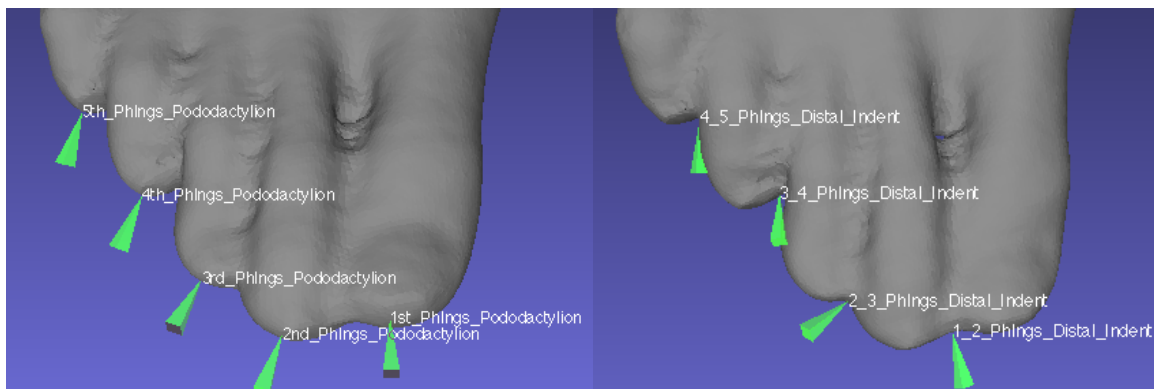
Figure 1. Points 1-8

Figure 2. Points 9-17 Podadactylion point found as if bringing a flat surface toward the toe.
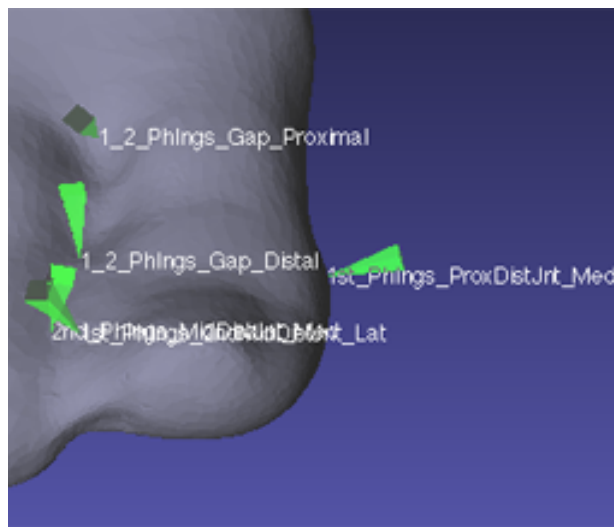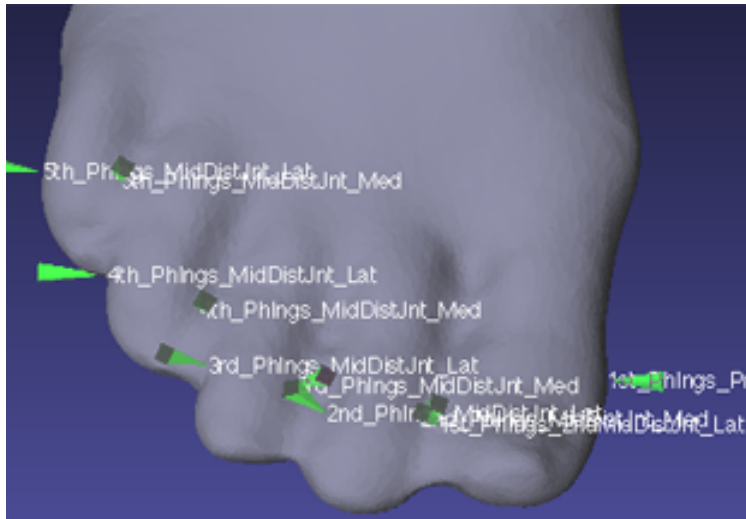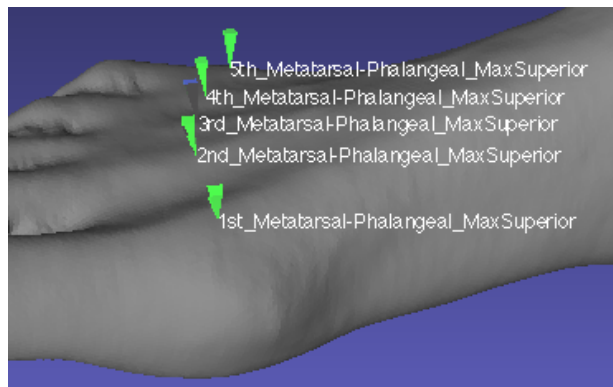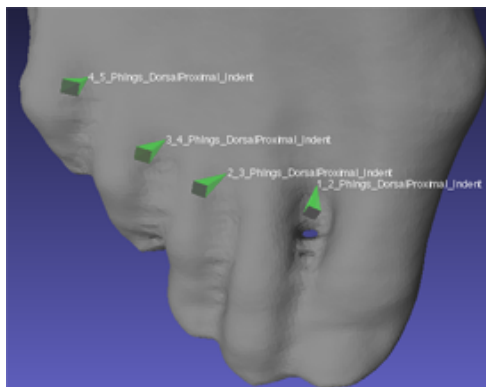
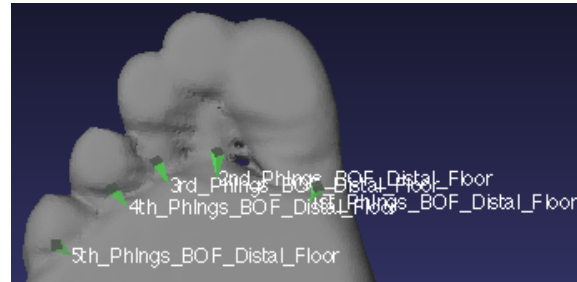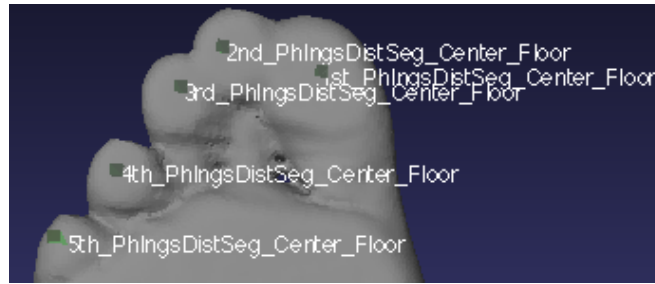Figure 3. Points 18-27 (See Table 2 for more information)
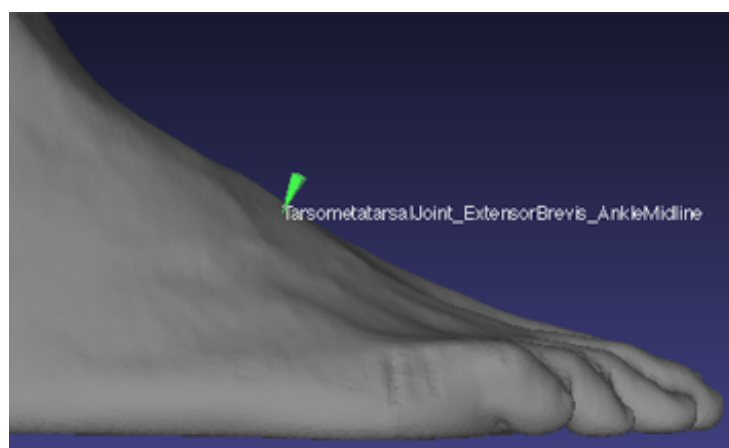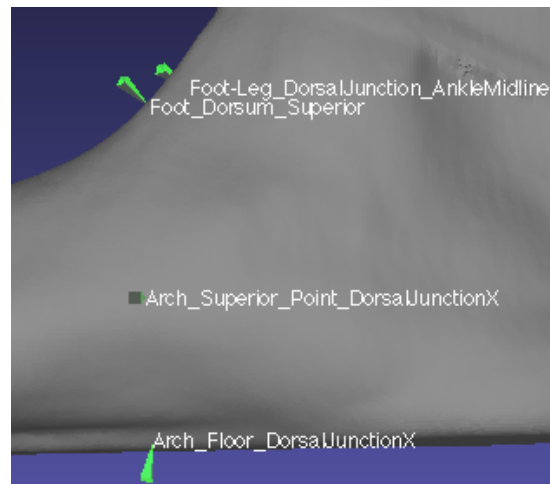

Figure 4. Points 30-38

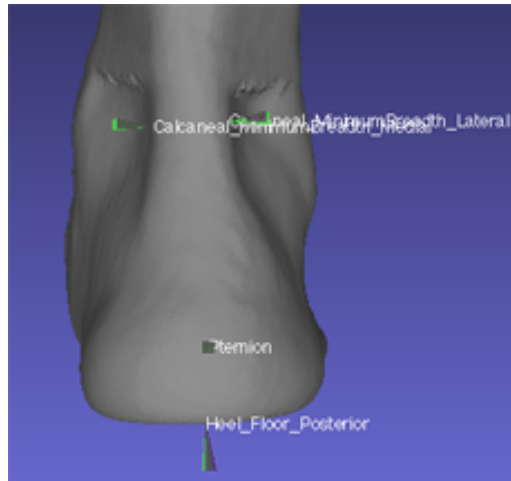Figure 5. Points 39-48

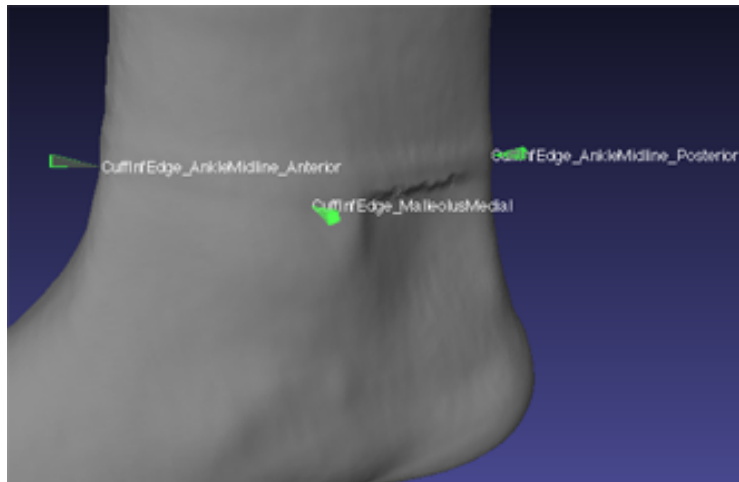Figure 6. Points 49-53

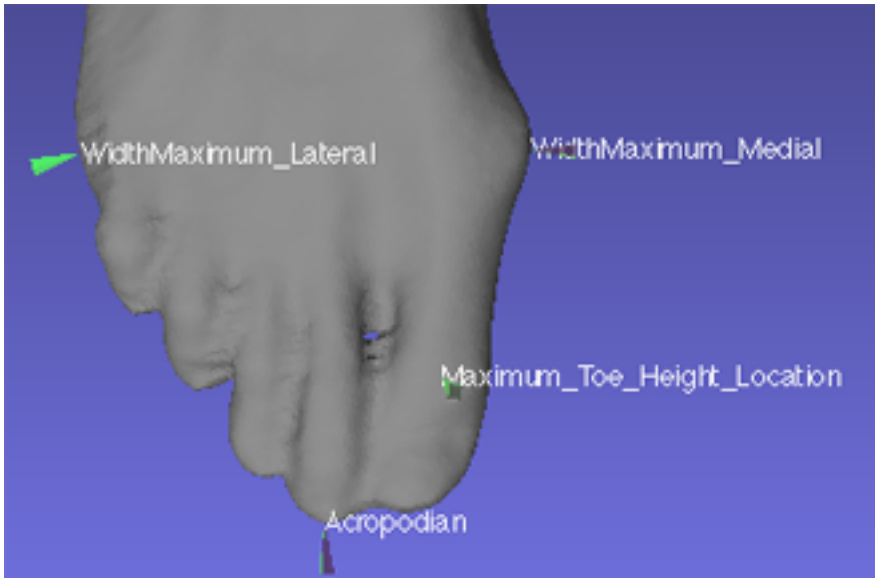Figure 7. Point 54-57

Figure 8. Points 58-61.

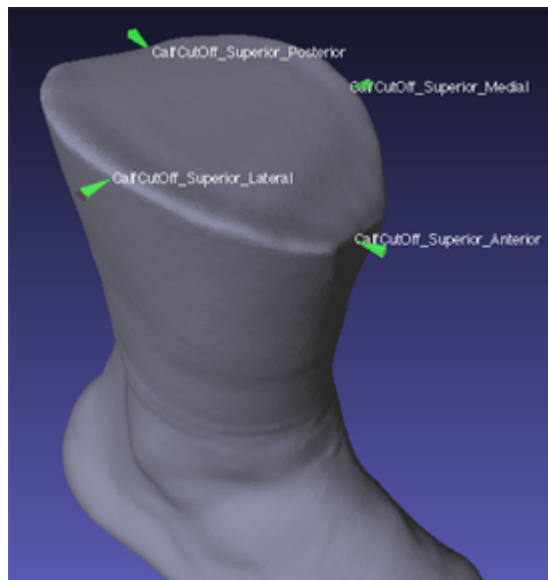Figure 9. Points 62-65(points whose change in location on the foot will disrupt template).
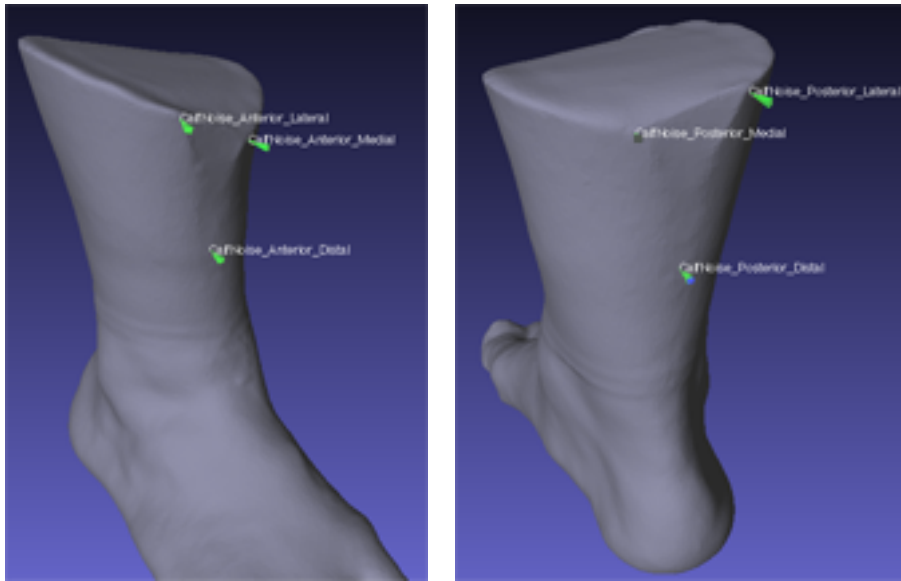

Figure 10. Points 66-69.

Figure 11. Points 70-75

APPENDIX B

Midsize Male Landmark Locations

Landmark	X	Y	Z
AnkleJoint	58.5	80.7	67.5
Malleolus_Lateral	57.9	79.2	74.1
Sphyrion_Fibulare	59.0	82.2	60.8
Malleolus_Medial	76.2	151.0	90.4
Sphyrion_Tibulare	77.3	149.9	77.6
1st_Metatarsal-Phalangeal_Protrsn	204.0	149.6	26.6
1st_Metatarsal-Phalangeal_Protrsn_Floor	202.6	141.1	4.5
1st_Phlngs_Pododactylion	274.0	124.1	17.7
2nd_Phlngs_Pododactylion	268.8	97.7	11.2
3rd_Phlngs_Pododactylion	257.0	81.5	10.7
4th_Phlngs_Pododactylion	241.3	68.7	10.7
1_2_Phlngs_Distal_Indent	245.7	113.9	17.5
2_3_Phlngs_Distal_Indent	257.7	89.4	11.4
3_4_Phlngs_Distal_Indent	242.7	75.2	11.5
4_5_Phlngs_Distal_Indent	224.0	61.8	13.2
4th_Phlngs_MidDistJnt_Lat	227.9	62.4	14.5
4th_Phlngs_MidDistJnt_Med	232.2	75.8	20.8
3rd_Phlngs_MidDistJnt_Lat	242.9	76.5	15.0
3rd_Phlngs_MidDistJnt_Med	247.2	90.8	19.3
2nd_Phlngs_MidDistJnt_Lat	254.5	91.8	16.6
2nd_Phlngs_MidDistJnt_Med	257.7	109.1	18.1
1st_Phlngs_2ndMidDistJnt_Lat	257.7	113.3	18.4
1_2_Phlngs_DorsalProximal_Indent	223.1	116.4	28.6
2_3_Phlngs_DorsalProximal_Indent	223.4	95.6	27.9
3_4_Phlngs_DorsalProximal_Indent	213.2	82.1	27.7
4_5_Phlngs_DorsalProximal_Indent	196.6	67.3	27.6
1st_Metatarsal-Phalangeal_MaxSuperior	205.9	131.2	41.7
2nd_Metatarsal-Phalangeal_MaxSuperior	212.4	104.4	32.9
3rd_Metatarsal-Phalangeal_MaxSuperior	206.8	90.6	31.7
4th_Metatarsal-Phalangeal_MaxSuperior	196.9	76.4	30.5
5th_Metatarsal-Phalangeal_MaxSuperior	179.8	61.5	28.5
1st_PhlngsDistSeg_Center_Floor	250.0	128.9	4.6
2nd_PhlngsDistSeg_Center_Floor	258.3	99.9	4.7
3rd_PhlngsDistSeg_Center_Floor	247.5	85.2	4.7
4th_PhlngsDistSeg_Center_Floor	232.5	72.7	4.9
5th_PhlngsDistSeg_Center_Floor	213.6	62.8	5.5
1st_Phlngs_BOF_Distal_Floor	221.7	131.5	4.5
2nd_Phlngs_BOF_Distal_Floor	225.5	103.8	4.4

3rd_Phlngs_BOF_Distal_Floor	220.3	89.9	4.5
4th_Phlngs_BOF_Distal_Floor	207.6	76.6	4.6
5th_Phlngs_BOF_Distal_Floor	194.4	64.2	4.8
Foot-Leg_DorsalJunction_AnkleMidline	120.6	111.2	83.0
Foot_Dorsum_Superior	127.3	110.5	78.2
Arch_Superior_Point_DorsalJunctionX	123.8	148.6	28.9
Arch_Floor_DorsalJunctionX	123.3	104.9	4.2
TarsometatarsalJoint_ExtensorBrevis_Midline	169.4	106.0	54.5
Heel_Floor_Posterior	16.5	114.9	4.2
Pternion	3.8	115.4	26.9
Calcaneal_MinimumBreadth_Medial	22.7	127.7	85.4
Calcaneal_MinimumBreadth_Lateral	21.0	108.7	85.2
Acropodian	274.2	121.0	16.9
WidthMaximum_Medial	202.7	150.6	20.1